Journal of Power Sources 187 (2009) 356–362

Contents lists available at ScienceDirect

Journal of Power Sources

journal homepage: www.elsevier.com/locate/jpowsour

Performance studies of solid oxide fuel cell cathodes in the presence of bare and cobalt coated E-brite alloy interconnects

Xuguang Li, Jong-Won Lee, Branko N. Popov*

Center for Electrochemical Engineering, Department of Chemical Engineering, University of South Carolina, Columbia, SC 29208, USA

ARTICLE INFO

Article history:
Received 15 September 2008
Received in revised form 30 October 2008
Accepted 5 November 2008
Available online 17 November 2008

Keywords:
Solid oxide fuel cell
Metallic interconnect
Co coating
Electroless deposition
Electrodeposition

ABSTRACT

The electrochemical performances of $La_{0.6}Sr_{0.4}Co_{0.2}Fe_{0.8}O_3$ (LSCF) electrodes were studied by half-cell measurements in the absence of chromia-forming alloy, in the presence of bare and Co coated E-brite alloy interconnects, respectively. The surface and cross-section properties of the bare and Co coated E-brite alloys, and LSCF electrodes were characterized by scanning electron microscopy (SEM), energy dispersive X-ray (EDX) analysis, and electron probe microanalysis (EPMA). The results showed a rapid degradation in LSCF performance when the bare E-brite alloy was used as interconnect. The growth of chromia scale on the E-brite alloy and the increase of Cr content throughout the LSCF electrode were observed. The uniform and dense Co coating process was developed to coat the E-brite alloy by using both electroless and electrodeposition methods. It was demonstrated that the Co layer effectively mitigates the Cr migration, leading to improved electrochemical stability of LSCF electrodes.

1. Introduction

In recent years, the intermediate temperature solid oxide fuel cell (SOFC) operating at 600–800 °C have attracted much interest, which makes high-temperature oxidation resistant alloys become possible to be used as interconnect in SOFC stack instead of traditional ceramic materials. Chromia-forming ferritic stainless steels are considered among the most promising candidate alloys for interconnects due to their high electronic and heat conductivities, low cost, easy fabrication, and appropriate thermal expansion behavior [1–3]. However, the exposure of these alloys to the oxidant atmosphere at high temperature can cause the formation of chromia scales, such as Cr_2O_3 which leads to a severe degradation in the cathode performance of SOFC due to the poisoning effect of chromium species. In detail, at high temperatures, the $CrO_2(OH)_2$ vapor is generated from the oxide scales on the chromia-forming ferritic alloys [4]:

$$Cr_2O_3 + (3/2)O_2 + 2H_2O \rightarrow 2CrO_2(OH)_2(g) \quad (1)$$

Since the oxygen partial pressure at the interface between the cathode and the electrolyte is lowered by electrode polarization, the $CrO_2(OH)_2$ vapor is reduced electrochemically during oxygen reduction, resulting in Cr_2O_3 precipitation:

$$2CrO_2(OH)_2(g) + 6e^- \rightarrow Cr_2O_3(s) + 2H_2O(g) + 3O^{2-} \quad (2)$$

This process causes an increase in the cathode charge transfer and diffusion resistance thereby leading to increase in the cell overvoltage with time. The Cr precipitates reduce the number of electrochemically active sites for oxygen reduction, leading to the long-term performance degradation of SOFC cathodes. The reduction rate of $CrO_2(OH)_2$ vapor and the nature of Cr species precipitated also depend on the cathode composition [5].

Oxygen reduction on (La,Sr)(Co,Fe)O_3 (LSCF) may proceed via three reaction paths [6]: (i) electrode surface path, (ii) electrode bulk path, and (iii) electrolyte surface path. According to these mechanisms, the electrochemically active sites for oxygen reduction extend from the three phase boundary (among the electrode, electrolyte and gas) to the electrode and electrolyte surfaces. The $CrO_2(OH)_2$ vapor reduction is a competing reaction with oxygen reduction, and thus its rate and consequently the degree of Cr poisoning strongly depends on the overpotential, the number of the catalytic sites and the geometric parameters of the porous cathode such as porosity and surface area.

In order to mitigate the chromium poisoning effect, much efforts have been made to develop protection layers on the metallic interconnect as a barrier to prevent chromium migration. A variety of coatings [7–24], such as $Mn_{1.5}Co_{1.5}O_4$ spinel, $La_{0.67}Sr_{0.33}MnO_3$ perovskite, $LaCrO_3$, Co, Ni, Cu, SmCo, Cr–Al–Y–O/Mn–Co–O, Mn–Co alloys, Y/Co have been prepared by thermal growth, sputtering, filtered arc deposition, chemical vapor deposition, and electroplating methods. The physical and chemical properties of the coated interconnects, such as electrical conductivity, surface stability, and microstructure and composition have been extensively investigated. However, to our knowledge, very few studies have been

* Corresponding author. Tel.: +1 803 777 7314; fax: +1 803 777 8265.
E-mail address: popov@engr.sc.edu (B.N. Popov).

0378-7753/$ – see front matter © 2008 Elsevier B.V. All rights reserved.
doi:10.1016/j.jpowsour.2008.11.018

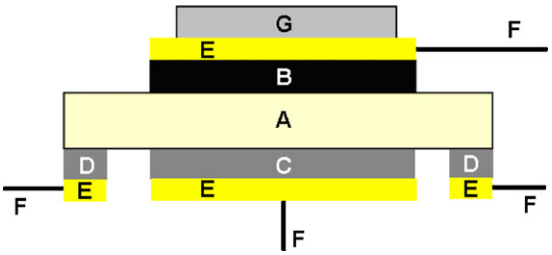

Fig. 1. Schematic diagram of half-cell configuration: (A) electrolyte, (B) working electrode, (C) counter electrode, (D) reference electrode, (E) Au current collector, (F) Au wire, and (G) E-brite alloy interconnect.

reported regarding the long-term electrochemical performances of SOFC cathodes in the presence of the bare and coated metallic interconnects.

In this work, the electrochemical stability of LSCF cathode were investigated by half-cell measurement in the presence of bare and Co coated E-brite alloy interconnect. For comparison, the LSCF performance without chromium source effect was also presented. The Co coating on E-brite alloy was developed by electroless deposition and electrodeposition methods, respectively. The scanning electron microscopy (SEM), energy dispersive X-ray (EDX), and electron probe microanalysis (EPMA) techniques were carried out to characterize the surface and cross-section properties of the interconnects and the electrodes.

2. Experimental

2.1. Electrochemical measurements

The half-cell configuration used in this work was shown in Fig. 1. An Y_2O_3-stabilized ZrO_2 (YSZ) pellet was used as the electrolyte. The thickness of the YSZ pellet is approximately 300 μm. A slurry of $La_{0.6}Sr_{0.4}Co_{0.2}Fe_{0.8}O_3$ (LSCF) was coated on one side of the YSZ pellet using a screen printing method, followed by sintering in air at 1100 °C for 2 h. The coated LSCF electrode has a porous structure and the electrode thickness is approximately 26 μm. The counter and the reference electrodes were prepared by brushing conductive Pt paste on the other side of the YSZ pellet, followed by firing in air at 1000 °C for 2 h. To provide electrical conduction, Au meshes and wires were attached to all electrodes. To study the extent of Cr poisoning on the cathode, an E-brite alloy (wt%, balance Fe, 27 Cr, 0.01 Mn) specimen was placed onto the Au mesh current collector of the working electrode. This design helps to prevent a direct solid-state reaction between the LSCF electrode and the interconnect as well as a significant degradation of cell performance resulting from the decrease in the electrical conductivity of the interconnect.

Moist air was supplied to the cell by passing the air through a water bubbler. Electrochemical measurements were performed using an EG&G PAR model 273 potentiostat. All experiments were conducted at 800 °C and at ambient pressure.

2.2. Preparation of cobalt coating on E-brite alloy interconnect

2.2.1. Electroless deposition [25–27]

Prior to cobalt coating, the E-brite alloy was activated in solution of 20 g L^{-1} sodium hypophosphite at 90 °C. Subsequent to activation the deposition was carried out with moderate stirring at 80–85 °C in 20 g L^{-1} cobalt sulfate, 20 g L^{-1} sodium hypophosphite, 50 g L^{-1} sodium citrate and 40 g L^{-1} ammonium chloride for 1 h. In addition to the above constituents, NH_4OH was added periodically during deposition to maintain the pH between 8.5 and 9.5. The pH was dropped below 9.0 frequently during deposition indicating that cobalt deposition on the alloy surface was proceeding. The deposition was terminated when the pH remained constant indicating the absence of cobalt in the solution. The resultant Co coated E-brite alloy was rinsed with deionized water, dried at 65 °C for 4 h and later sintered at 1000 °C in H_2 for 4 h.

2.2.2. Electrodeposition

The electroplating solution was carried out according to a modified procedure [8]. 137 g of $CoSO_4{\cdot}7H_2O$ and 33 g of $CoCl_2{\cdot}6H_2O$, 6.2 g of H_3BO_3 was dissolved in 500 g of distilled water. Prior to electroplating, the E-brite substrate was rinsed with plenty of water and then electrochemically etched at 1.0 mA cm^{-2} in the electroplating solution. Electrodeposition was done at a current density of 10.0 mA cm^{-2}. The coated samples were sintered at 1000 °C in H_2 for 4 h.

2.3. Physical and chemical characterizations

SEM (FEI Quanta 200) and EDX analysis were used to obtain the cross-section and surface morphologies as well as elemental contents of the LSCF electrodes and interconnects, respectively. EPMA (Cameca Instrument SX50) was performed to observe the distribution profile of elements on the interconnects.

3. Results and discussion

3.1. Electrochemical performances of LSCF electrodes in the absence and presence of bare E-brite alloy interconnect

Fig. 2a shows the potential transients of LSCF electrode as a function of time measured at current density of 200 mA cm^{-2} at 800 °C in the absence and presence of the bare E-brite alloy interconnect. It can be seen that, when the cell was operated without chromia-forming ferritic alloy interconnect, the LSCF electrode exhibited a slow decrease in the performance with time. Similar phenomena were also observed by Kim et al. for the SOFC with LSCF cathode operated with no Cr source at 750 °C [28]. Moreover, as shown in Fig. 2, when a bare E-brite alloy interconnect was applied, the electrochemical performance of LSCF electrode significantly decreases with time. In addition, it was found that, the performance loss of LSCF electrode can be at least partially recovered upon current interruption, indicating that the total performance loss consists of "reversible" and "irreversible" losses. However, when the current was switched on, the overpotential increases again with time. The surface enrichment of a secondary phase, such as SrO on the LSCF can result in the observed decrease of the cell performance. The initial performance enhancement of the restarted cell is attributed to the removal or incorporation of surface SrO species into LSCF lattice [29]. According to the literatures [1–3] and our results, the severe electrochemical performance degradation of LSCF cathode is also attributed to the Cr poisoning effect on LSCF electrode via the vaporization of gaseous Cr species from the Cr oxide scale under oxidizing conditions. This will be further demonstrated by the SEM, EDX, and EPMA characterization of metallic interconnects and electrodes in the following section.

Fig. 2b shows the polarization curves measured before stability testing and after 400 h operation in the absence and presence of the bare E-brite alloy interconnect. In the presence of bare E-brite alloy, the initial polarization performance of LSCF electrode is much lower than that without Cr source. The severe performance degradation was observed for the former after 400 h operation. This is consistent with the chronopotentiometric stability testing result.

Fig. 3a shows the SEM image of the cross-section of the bare E-brite alloy interconnect after oxidation in air at 800 °C for 400 h. It is evident that the interconnect was covered with an oxide scale

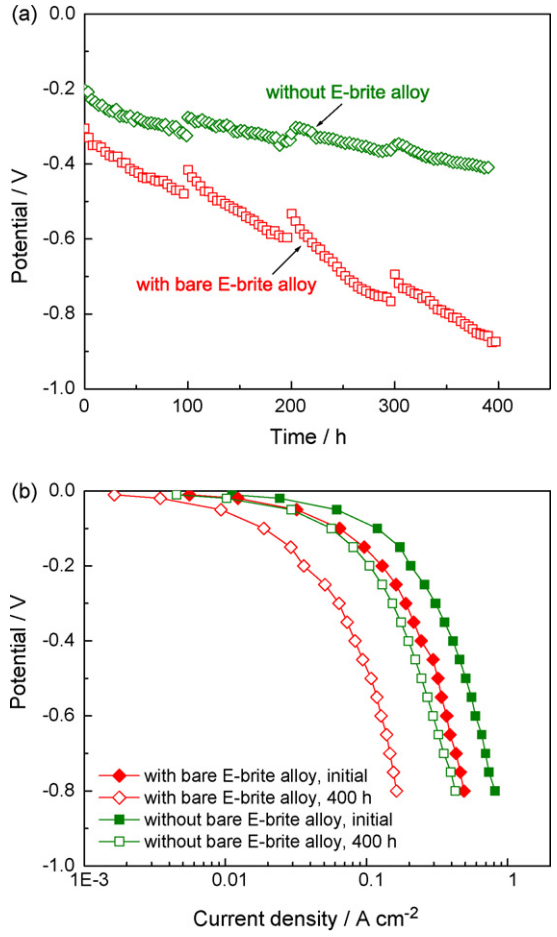

Fig. 2. (a) Potential transients of LSCF electrodes as a function of time measured at current density of 200 mA cm^{-2} in the absence and presence of the bare E-brite alloy interconnect. (b) Polarization curves of LSCF electrodes measured before stability testing and after 400 h operation in the absence and presence of the bare E-brite alloy interconnect. The experiments were performed at 800 °C in air.

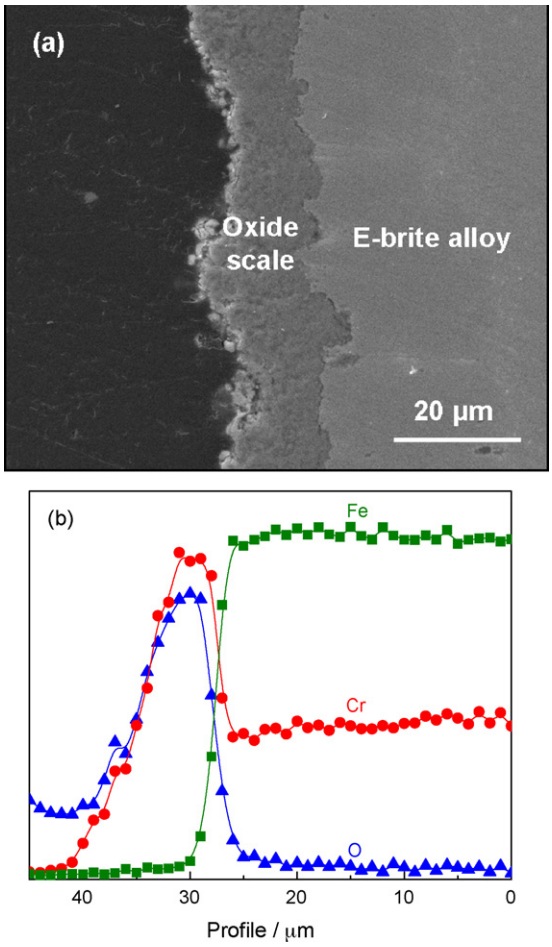

Fig. 3. (a) SEM image of the cross-section of the bare E-brite alloy interconnect after oxidation in air at 800 °C for 400 h. (b) EPMA profiles of Fe, Cr and O in the bare E-brite alloy interconnect after oxidation in air at 800 °C for 400 h.

layer with the thickness of approximately 13 μm. In particular, the scale layer becomes brittle and porous after long-term operation. EPMA was used to determine the oxide scale on the surface of E-brite alloy, and the result is presented in Fig. 3b. It can be seen that, Cr and O are enriched in the scale layer formed on the interconnect surface. This indicated that during long-term stability testing, Cr diffuses from the bulk of the alloy toward the alloy surface, leading to the continuous formation of Cr oxide layer.

Fig. 4 presents the SEM image of the cross-section of the half-cell (i.e., LSCF coated on YSZ) after 400 h stability testing in air at 800 °C. The Cr content was determined by using EDX analysis in the different regions as indicated in Fig. 4. As shown in Table 1, after 400 h operation in air at 800 °C, the Cr content in the half-cell gradually increases from the surface of LSCF electrode to the interface of LSCF/YSZ, and a maximum Cr content was found at the interface between the LSCF electrode and the YSZ electrolyte (Region 2).

In this study, the E-brite alloy was physically separated from the LSCF electrode by Au mesh and Au paste, and hence Cr

Table 1
EDX analysis of Cr content (wt%) in the LSCF electrode operated with the bare E-brite alloy and the Co coated E-brite alloy interconnects prepared by electroless deposition and electrodeposition methods, respectively. The analysis was conducted on the selected areas as indicated in Fig. 4.

Interconnect	1	2	3	4	5
Bare E-brite alloy	0.57	9.35	5.56	3.26	2.63
Co coated E-brite prepared by electroless deposition	0.18	0.51	0.37	0.33	0.29
Co coated E-brite alloy prepared by electrodeposition	0.22	0.82	0.56	0.44	0.41

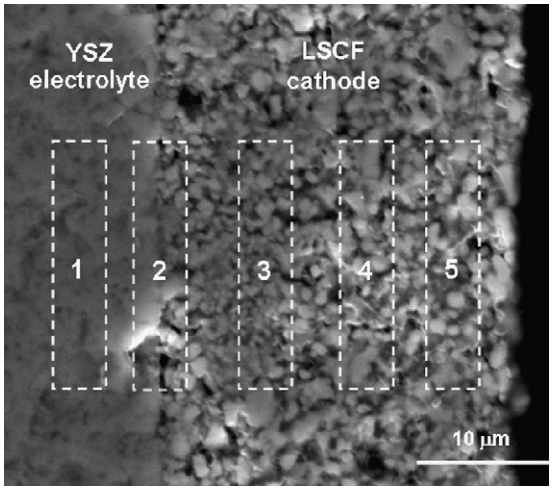

Fig. 4. SEM image of the cross-section of the half-cell (LSCF/YSZ) after 400 h stability testing in air at 800 °C.

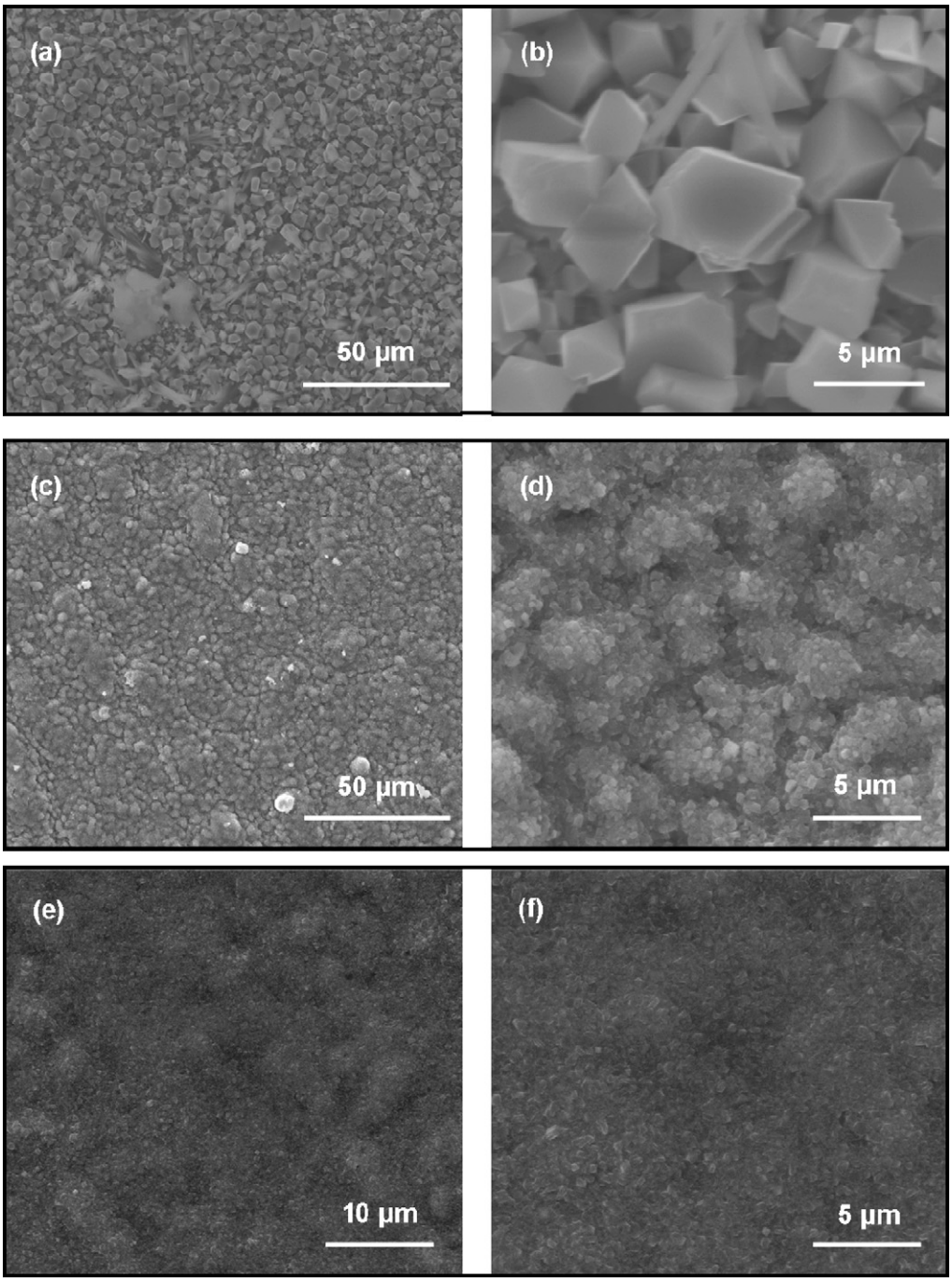

Fig. 5. SEM images of surface morphologies of (a and b) bare E-brite alloy, (c and d) Co coated E-brite alloy prepared by electroless deposition method and (e and f) Co coated E-brite alloy prepared by electrodeposition method after oxidation in air at 800 °C for 400 h.

poisoning only occurs via vapor phase transport rather than a solid-state reaction. The $CrO_2(OH)_2$ vapor is generated from the oxide scales on the E-brite alloy interconnect (see Fig. 4), and it is reduced electrochemically during oxygen reduction. Since LSCF exhibits a mixed conducting property, both the LSCF/YSZ interface and the LSCF surface serve as the electrochemically active sites for oxygen reduction. Therefore, Cr precipitation was observed not only at the LSCF/YSZ interface, but also throughout the LSCF cathode layer. The Cr precipitation may cause the irreversible loss of LSCF activity observed in Fig. 2, by reducing the number of electrochemically active sites for oxygen reduction.

3.2. Development of Co coatings on E-brite alloy by electroless deposition and electrodeposition methods

Electroless deposition method has been extensively studied in our group to deposit Co on the AB_4 type hydrogen storage alloys and the NiO cathode of molten carbonate fuel cell [25–27]. It provides a reliable way to coat substrate with uniform and dense Co layer. The resultant Co coating effectively improves the stability of substrates in electrochemical and high-temperature environments. In this work, electroless and electrodeposition methods were used to prepare Co protection layer on E-brite alloy for SOFC interconnect application.

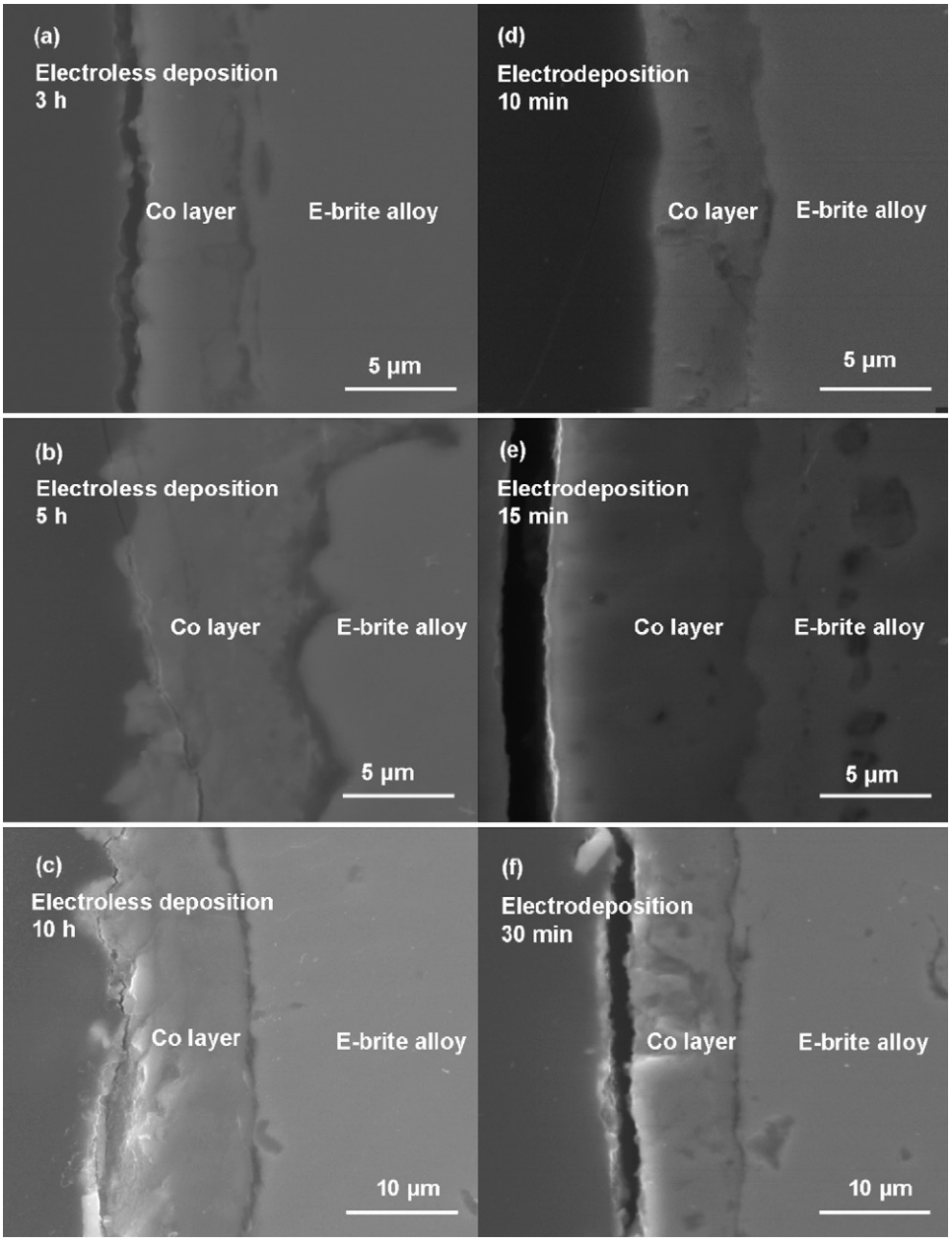

Fig. 6. SEM images of the cross-sections of the Co coated E-brite alloys prepared by (a–c) electroless deposition and (d–f) electrodeposition methods with different deposition times, respectively, after oxidation in air at 800 °C for 400 h.

Fig. 5 shows the SEM images of the surface morphologies of the bare E-brite alloy, and Co coated E-brite alloys after oxidation in air at 800 °C for 400 h prepared by electroless deposition and electrodeposition methods. It can be seen from Fig. 5a (low magnification) and b (high magnification) that, the oxide scale formed on the bare E-brite alloy exhibits a rough and porous surface and is composed of angular chromium oxide crystals with the diameters ranging from several hundreds of nanometers to several micrometers. EDX analysis indicated that it contains about 53.8 wt% Cr, which means the enrichment of Cr in the oxide scale. In contrast, Fig. 5c (low magnification) and d (high magnification) showed that, the electroless deposited Co protection layer over E-brite alloy is dense and compact. It composes of uniform agglomerates containing smaller Co crystalline with the average particle size of approximately 200 nm. EDX analysis indicated that it consists of about 2.1 wt% Cr and 74.4 wt% Co. This means that the Co protection layer greatly decrease the Cr diffusion. As shown in Fig. 5e (low magnification) and f (low magnification), the electrodeposited Co layer is as dense and compact as the electroless deposited sample. Moreover, it is more even with smaller cluster composing of cobalt crystalline with average particle size of 100–200 nm. It contains about 3.4 wt% Cr and 68.9 wt% Co, which is comparable with the electroless deposited Co layer.

Fig. 6 shows the SEM images of the cross-sections of Co coated E-brite alloy prepared by electroless deposition and electrodeposition methods with different deposition times, respectively, after oxidation in air at 800 °C for 400 h. As shown in Fig. 6a–c, the thicknesses of Co layers prepared by electroless deposition method can be controlled in the range of 5–12 μm by changing deposition times from 3 to 10 h. Similar phenomena were also observed for the electrodeposition method by which the Co layer

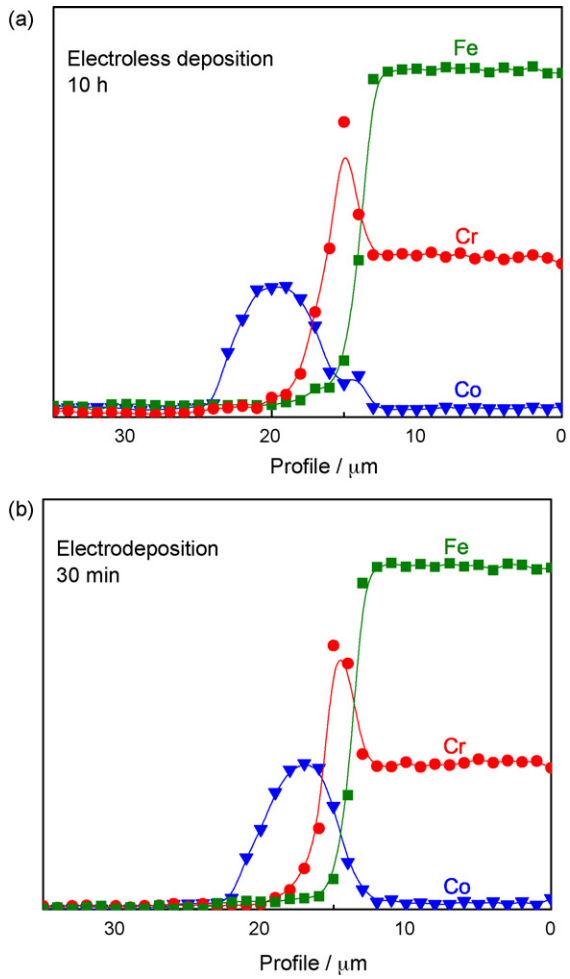

Fig. 7. EPMA profiles of Fe, Cr, Co and O in the Co coated E-brite alloys prepared by (a) electroless deposition method for 10 h and (b) electrodeposition for 30 min, respectively, after oxidation in air at 800 °C for 400 h.

thickness was varied from 4 to 10 μm with deposition times of 10–30 min (see Fig. 6d–f). The cross-sectional SEM images further demonstrate the dense and compact structures of the Co protection layers. Compared to the porous coating layer prepared with traditional slurring coating method [23], the electroless deposited and electrodeposited Co coating layers more efficiently hinder the migration of Cr species. In addition, in comparison with the bare E-brite alloy, no distinct Cr oxide scale layer can be identified for the Co coated E-brite alloy samples from the SEM cross-section images. Furthermore, Fig. 7 presents the EPMA analysis of elemental distributions in the Co coated E-brite alloys prepared by electroless deposition and electrodeposition methods with deposition times of 10 h and 30 min, respectively. The result indicated that the Co layer and Cr layer can inter-diffuse after oxidation in air at 800 °C for 400 h. That is, there is an interface layer consisting Co–Cr–O between E-brite substrate and Co coating. It may also consist of mixed spinel phases containing $CoCrFeO_4$, Co_2CrO_4, $CoCr_2O_4$ (conductivity: ~1.96 S cm^{-1} at 750 °C) and Co_3O_4 (conductivity: ~35.5 S cm^{-1} at 750 °C) [8,30]. This means that both electroless deposited and electrodeposited Co protection layers can effectively mitigate the Cr outward diffusion. It has been reported that the Co layer has conductivity of 6–7 S cm^{-1} at 800 °C, two orders of magnitude higher than Cr_2O_3 [31]. This may also be beneficial to the performance improvement of practical SOFC stack.

3.3. Electrochemical performances of LSCF electrode in the presence of Co coated E-brite alloy interconnects

Fig. 8a compares the potential transients of LSCF cathode as a function of time at current density of 200 mA cm^{-2} in the presence of Co coated E-brite alloy interconnects. Fig. 8b shows the polarization curves measured before stability testing and after 400 h operation in the presence of the Co coated E-brite alloy interconnects. The experiments were performed at 800 °C. The cell performance operated in the presence of the bare E-brite alloy was also presented for comparison. As shown in Fig. 8, in comparison with the continuous performance degradation of the LSCF electrode operated with the bare metallic interconnect, the cell with the Co coated interconnects showed much more slow performance degradation with time. As can be seen in Table 1, after 400 h operation in air at 800 °C with the Co coated interconnects, the Cr content throughout the LSCF/YSZ is only around 0.5 wt%, which is much lower than that in the presence of E-brite alloy interconnect. This indicated that a dense Co coating effectively reduces the amount of $CrO_2(OH)_2$ vapor generated from the E-brite alloy interconnect and transported to the LSCF/YSZ interface, thus decreasing the Cr poisoning rate of the LSCF cathode. Moreover, the electroless deposited Co coating exhibits slightly higher performance than the electrodeposited counterpart. This may be due to the higher Co layer thickness of the former or/and the higher stability of electroless deposited Co in the high-temperature and electrochemical environ-

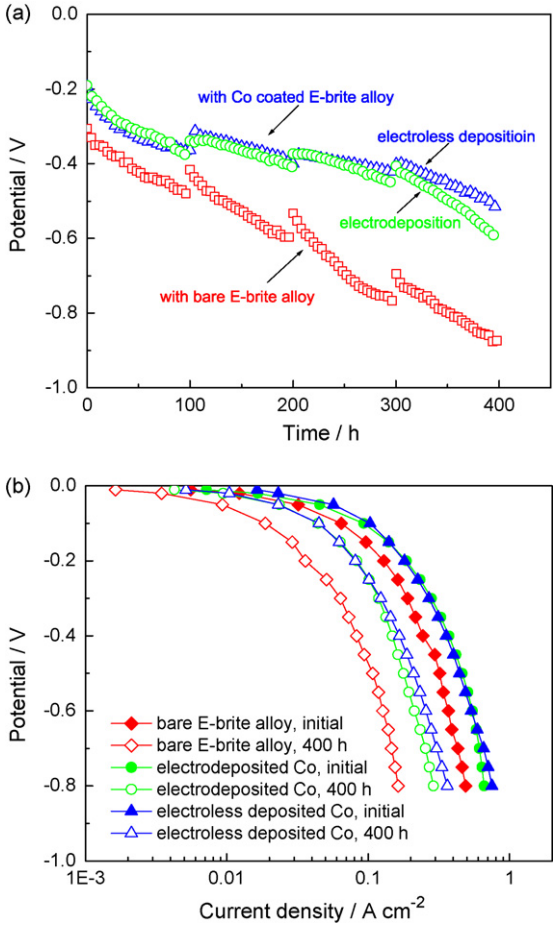

Fig. 8. (a) Potential transients of LSCF electrodes as a function of time measured at current density of 200 mA cm^{-2} in the presence of bare and Co coated E-brite alloy interconnects. (b) Polarization curves of LSCF electrodes measured before stability testing and after 400 h operation in the presence of the bare and Co coated E-brite alloy interconnects. The experiments were performed at 800 °C in air.

ments [25–27]. In addition, the residual phosphorus element in the electroless deposited Co layer introduced by sodium hypophosphite may help to prevent the Cr outward diffusion. Another possible reason is that the structure of Co layer prepared by electroless deposition method is generally more amorphous than that prepared by electrodeposition method, which may also be beneficial for better long-term electrochemical stability.

4. Conclusions

The long-term performances of LSCF cathodes were studied in the presence of bare E-brite alloy interconnect. The loss of electrocatalytic activity of LSCF for oxygen reduction was evaluated in a half-cell as a function of time by applying a constant current density. The cathodic overpotential continuously increases with time, indicating the activity loss of LSCF in the presence of bare E-brite interconnect. The interconnects after oxidation in air at 800 °C for 400 h were found to be completely covered with a Cr-rich oxide scale layer. The characterization study indicated that Cr precipitation at the cathode/electrolyte interface as well as throughout the cathode causes the irreversible loss of LSCF activity, by reducing the number of electrochemically active sites for oxygen reduction. The efficient Co protective coatings were developed by electroless deposition and electrodeposition methods, respectively. The electrochemical stability study indicated that the resultant Co coatings act as an effective barrier for Cr migration, leading to an improved performance of LSCF cathodes.

Acknowledgment

Financial support provided by General Electric is acknowledged gratefully.

References

[1] W.Z. Zhu, S.C. Deevi, Mater. Sci. Eng. A 348 (2003) 227–243.
[2] Z. Yang, K. Scott Weil, D.M. Paxton, J.W. Stevenson, J. Electrochem. Soc. 150 (2003) A1188–A1201.
[3] S.P. Jiang, Solid State Ionics 146 (2002) 1–22.
[4] Y. Matsuzaki, I. Yasuda, Solid State Ionics 132 (2000) 271–278.
[5] Y. Matsuzaki, I. Yasuda, J. Electrochem. Soc. 148 (2001) A126–A131.
[6] J. Fleig, Annu. Rev. Mater. Res. 33 (2003) 361–382.
[7] Z. Yang, G. Xia, S.P. Simner, J. Stevenson, J. Electrochem. Soc. 152 (2005) A1896–A1901.
[8] X. Deng, P. Wei, M.R. Bateni, A. Petric, J. Power Sources 160 (2006) 1225–1229.
[9] M. Stanislowski, J. Froitzheim, L. Niewolak, W.J. Quadakkers, K. Hilpert, T. Markus, L. Singheiser, J. Power Sources 164 (2007) 578–589.
[10] D.E. Alman, C.D. Johnson, W.K. Collins, P.D. Jablonski, J. Power Sources 168 (2007) 351–355.
[11] Z. Lu, J. Zhu, Y. Pan, N. Wu, A. Ignatiev, J. Power Sources 178 (2008) 282–290.
[12] P.E. Gannon, C.T. Tripp, A.K. Knospe, C.V. Ramana, M. Deibert, R.J. Smith, V.I. Gorokhovsky, V. Shutthanandan, D. Gelles, Surf. Coat. Technol. 188–189 (2004) 55–61.
[13] P.E. Gannon, V.I. Gorokhovsky, M.C. Deibert, R.J. Smith, A. Kayani, P.T. White, S. Sofie, Z. Yang, D. McCready, S. Visco, C. Jacobson, H. Kurokawa, Int. J. Hydrogen Energy 32 (2007) 3672–3681.
[14] M. Reza Bateni, P. Wei, X. Deng, A. Petric, Surf. Coat. Technol. 201 (2007) 4677–4684.
[15] I. Belogolovsky, X.-D. Zhou, H. Kurokawa, P.Y. Hou, S. Visco, H.U. Anderson, J. Electrochem. Soc. 154 (2007) B976–B980.
[16] J. Wu, C. Li, C. Johnson, X. Liu, J. Power Sources 175 (2008) 833–840.
[17] J. Wu, Y. Jiang, C. Johnson, X. Liu, J. Power Sources 177 (2008) 376–385.
[18] W. Qu, L. Jian, D.G. Ivey, J.M. Hill, J. Power Sources 157 (2006) 335–350.
[19] Z. Yang, G.-G. Xia, G.D. Maupin, J.W. Stevenson, J. Electrochem. Soc. 153 (2006) A1852–A1858.
[20] Y. Larring, T. Norby, J. Electrochem. Soc. 147 (2000) 3251–3256.
[21] H. Kurokawa, C.P. Jacobson, L.C. DeJonghe, S.J. Visco, Solid State Ionics 178 (2007) 287–296.
[22] M. Stanislowski, E. Wessel, K. Hilpert, T. Markus, L. Singheiser, J. Electrochem. Soc. 154 (2007) A295–A306.
[23] J.-H. Kim, R.-H. Song, S.-H. Hyun, Solid State Ionics 174 (2004) 185–191.
[24] K. Fujita, K. Ogasawara, Y. Matsuzaki, T. Sakurai, J. Power Sources 131 (2004) 261–269.
[25] B.S. Haran, B.N. Popov, R.E. White, J. Electrochem. 145 (1998) 3000–3007.
[26] A. Durairajan, B.S. Haran, B.N. Popov, R.E. White, J. Power Sources 83 (1999) 114–120.
[27] A. Durairajan, H. Colon-Mercado, B. Haran, R. White, B. Popov, J. Power Sources 104 (2002) 157–168.
[28] J.Y. Kim, N.L. Canfield, L.A. ChickL, K.D. Meinhardt, V.L. Sprenkle, Progress in Solid Oxide Fuel Cells, Wiley, Hoboken, 2006, pp. 239–247.
[29] W. Wang, S.P. Jiang, Solid State Ionics 177 (2006) 1361–1369.
[30] W. Qu, L. Jian, J.M. Hill, D.G. Ivey, J. Power Sources 153 (2006) 114–124.
[31] H. Ling, A. Petric, in: S.C. Singhal, J. Mizusaki (Eds.), Proceedings of Symposium on Solid Oxide Fuel Cells IX, vol. 2005–07, The Electrochemical Society, Pennington, NJ, 2005, pp. 1866–1873.